Mechanisms of the rearrangement processes in the $dt\mu$ system: Nonadiabatic transitions and interference effects

V. N. Ostrovsky*
Institute of Physics, The University of St. Petersburg, St. Petersburg 198904, Russia
(Received 29 March 1999; revised manuscript received 16 September 1999; published 16 February 2000)

For the rearrangement process $d\mu(n_i)+t\to d+t\mu(n_f)$, results of high-precision numerical calculations for the zero total orbital momentum of the system are compared with those obtained from the analytical Demkov model. The latter is widely used in atomic collision theory to describe rearrangement processes with small energy defects. A specific feature of the studied system is that the energy defect has a purely isotopic nature. Muon transfer within the $n_i=n_f=1$ and $n_i=n_f=2$ manifolds is analyzed. In the latter case the natural reaction channels correspond to Stark states in the limit of separated atoms. Efficient transitions occur between Stark states with the muon cloud stretched toward (opposite to) the collision partner both in the initial and final states. An overall good agreement with accurate results sustains the relevance of the Demkov model for the studied process, and clarifies the reaction mechanisms. The interference effects strongly suppress the reaction probability within the $n_i=n_f=1$ manifold, and enhance it for $n_i=n_f=2$. Some intriguing although yet unexplained features of the interference phases are revealed and discussed: they are almost energy independent and close to integer multiples of $\frac{1}{2}\pi$.

PACS number(s): 36.10.Dr, 34.70.+e, 34.50.Pi

I. INTRODUCTION

The $dt\mu$ system is a particular case of a general three-body Coulomb system comprising one light particle and two heavy particles. In the present paper we consider rearrangement processes

$$d\mu(n_i)+t\to d+t\mu(n_f)+\Delta E \tag{1}$$

for zero total angular momentum. In recent years this system has attracted a considerable attention [1–14] due to its role in the muon-catalyzed fusion project [15]. In some of these papers numerically intensive calculations were carried out to produce high-precision results. Although the value of such information is difficult to overestimate, very often it does not contribute directly to improving our qualitative understanding of the collision dynamics, and one still has to look for interpretations of the calculated results in terms of some reaction mechanisms. This can be achieved by simplifying the problem at hand, and reducing it to one of the analytical models developed for a description of some generic physical situations. If such a simplification is possible, then a comparison of accurate numerical results with those obtained from the model analysis is useful and interesting because it facilitates a qualitative understanding of the former and, at the same time, examines the range of applicability of the latter.

We are interested in slow collisions when the most efficient transitions occur in a quasiresonance regime characterized by small values of the energy defect ΔE. This is the case when the principal quantum numbers in the initial (n_i) and final (n_f) bound states coincide, $n_i=n_f\equiv n$, and

$$\Delta E_n=E_{d\mu(n)}-E_{t\mu(n)}=\frac{m_{t\mu}-m_{d\mu}}{2n^2}, \tag{2}$$

where $E_{d\mu(n)}$ and $E_{t\mu(n)}$ are the energies of the bound states of the pairs $d\mu$ and $t\mu$, respectively, and $m_{d\mu}$ and $m_{t\mu}$ are the corresponding reduced masses:

$$m_{d\mu}=\frac{m_d m_\mu}{m_d+m_\mu}, \quad m_{t\mu}=\frac{m_t m_\mu}{m_t+m_\mu}. \tag{3}$$

Taking into account that $m_t\sim m_d\gg m_\mu$, we obtain

$$\Delta E_n=m_\mu^2\frac{m_t-m_d}{m_d m_t}\frac{1}{2n^2}\left[1+O\left(\frac{m_\mu}{m_d}\right)\right]. \tag{4}$$

Thus ΔE vanishes in the limit $m_\mu/m_d\to 0$ (or $m_\mu/m_t\to 0$) as well as in the limit $m_d/m_t\to 1$ that reveals isotopic nature of the energy defect.

Process (1) represents transfer of a light particle (muon) between two heavy ones (d and t). The semiclassical approach to this type of process is well developed in the theory of slow atomic collision. Here the light particle is an electron and the process is usually referred to as charge exchange or charge transfer. A two-state model for quasiresonance charge exchange was developed by Demkov [16]. Being closely related to the model proposed earlier in different context by Rosen and Zener [17], the Demkov model is much more flexible. It is widely applied to atomic collisions [18–23]; we also mention application to the theory of muon distribution among the fission fragments in mesic atoms [24,25,21]. The explicit time dependence of a two-state Hamiltonian in the Demkov model corresponds to a classical (or semiclassical) description of the motion of atomic nuclei. Remarkable progress in the generalization to account for a quantum description of this motion was subsequently achieved. Menshikov [26] managed to derive an exact quantum expression specifically for the nonadiabatic transition probability with-

*Electronic address: Valentin.Ostrovsky@pobox.spbu.ru

out actually solving the Schrödinger equation. Recently Osherov and Voronin [27] gave a complete solution to the two-state quantum problem. However, we consider collision energies much larger than the resonance defect ΔE; in this case the quantum effects are negligible, except in the near-threshold domains, and it is justified to use a semiclassical version of the Demkov model. It should be emphasized that it is not our aim here to elaborate upon the model approach to the highest level of sophistication; on the contrary, we prefer to keep it as simple as possible provided that it is capable of reproducing major features of the energy dependence of the reaction probability.

In ion-atom collisions the energy defect results from the difference of the effective potentials used to represent each of two atomic cores. Recently, based on the so-called hidden crossing theory, Janev [23] demonstrated the relevance of the Demkov model for a description of electron transfer between two bare nuclei. The energy defect in this case originates from the difference of the nuclear charges or/and the electron principal quantum numbers in the initial and final states. In our system the energy defect has an isotopic nature, as stressed above. However, notwithstanding this difference, application of the Demkov model remains rather straightforward in the case of ground-to-ground state charge exchange ($n_i=n_f=1$, Sec. II A). For excited states, the situation becomes more complicated due to the Coulomb degeneracy of the separated atom states, and the relevance of the two-state Demkov model is not evident. We consider in detail the $n_i=n_f=2$ manifold, and show that it can be split into two weakly coupled pairs of strongly interacting adiabatic channels. After that the system is approximately described by two independent two-state Demkov models (Sec. II B). The model results are successfully compared with the recent high-precision benchmark calculations by Tolstikhin and Namba [14] based on the hyperspherical method implemented in terms of hyperspherical elliptic coordinates [28] and the ''slow/smooth variable discretization method'' [29] in combination with the $\mathcal{R}$-matrix propagation technique of Ref. [30]. We find that interference effects play an important role for reaction (1), strongly suppressing the rearrangement probability for $n_i=n_f=1$ and enhancing it for $n_i=n_f=2$. In addition, the interference phases exhibit some unexpected behavior discussed in Sec. III.

II. MODELS

A. Ground-to-ground state rearrangement

In the Demkov model, *diabatic* states correspond to the atomic orbitals of separated atoms split by the energy ΔE. The coupling of these states $H_{ab}(R)$ is induced by the electron exchange between the centers, and decreases exponentially with increasing internuclear distance R. *Adiabatic* (quasimolecular) states coincide with diabatic ones for $R\to\infty$. For small R [where $H_{ab}(R)\gg\Delta E$], the quasimolecular adiabatic states represent linear combinations of atomic states with almost equal weights. The states rearrange from an atomic to a molecular pattern, and related strong nonadiabatic transitions occur in the vicinity of the point R_c defined by the condition

$$\Delta E=2H_{ab}(R_c). \tag{5}$$

For a single passage of the strong-coupling region, the probability of a transition between adiabatic (quasimolecular) states is

$$p=\left[1+\exp\left(\frac{\pi\Delta E}{\alpha v}\right)\right]^{-1}. \tag{6}$$

In the simplest approximation [cf. Eq. (21) below], v is the collision velocity related to the center-of-mass collision energy $E_{\rm col}$:

$$v=\sqrt{\frac{2E_{\rm col}}{\mathcal{M}_i}}. \tag{7}$$

In our case the relevant mass $\mathcal{M}_i$ is

$$\mathcal{M}_i=\frac{m_{d\mu}m_t}{m_{d\mu}+m_t}. \tag{8}$$

Hereafter, unless stated otherwise, we use a muonic system of units ($\hbar=e=m_\mu=1$), although we sometimes retain muonic mass m_μ in the formulas. The parameter α characterizes the exponential behavior of the exchange coupling $H_{ab}(R)$ at large separations. The theory asymptotic in large internuclear (i.e., $d-t$) separation R (for a review see Ref. [31]), gives for the coupling $H_{ab}(R)$ in the case of Σ states of a quasimolecule,

$$H_{ab}(R)=4\pi R2^{Z_a/\alpha_a+Z_b/\alpha_b-3}\times\exp\left(-\frac{Z_a}{2\alpha_a}-\frac{Z_b}{2\alpha_b}\right)\psi_a\left(\frac{1}{2}R\right)\psi_b\left(\frac{1}{2}R\right), \tag{9}$$

where α_a and α_b are related to the initial- and final-state binding energies E_a and E_b for $d\mu$ and $t\mu$ systems, respectively: $\alpha_a=\sqrt{2m_{d\mu}E_a}$ and $\alpha_b=\sqrt{2m_{t\mu}E_b}$. The label $a(b)$ is attached hereafter to the initial (final) state of process (1), and to the adiabatic quasimolecular potential curve which is correlated to it.

The wave functions ψ_a and ψ_b describe initial and final (separated atom) states, respectively. They decrease exponentially at large distances from the nucleus: $\psi_j(r)\sim\exp(-\alpha_j r)$. Therefore $H_{ab}(R)\sim\exp[-1/2(\alpha_a+\alpha_b)R]$, and one have insert $\alpha=1/2(\alpha_a+\alpha_b)$ into Eq. (6). The wave functions ψ_a and ψ_b actually depend on the electron vectors; by writing $\psi_a(\frac{1}{2}R)$ and $\psi_b(\frac{1}{2}R)$ in Eq. (9), we imply that these functions are to be evaluated at the midpoint between the atomic nuclei. Formula (9) is derived for the space-fixed (i.e., infinitely heavy) atomic nuclei separated by a distance R. Therefore it is consistent to neglect in it the isotopic effects that give $\alpha_a\approx\alpha_b\approx 1/n$. This approximation is sufficient for an evaluation of the parameter α in formula (6): $\alpha=1/n$. This completes the parametrization of the probability p [Eq. (6)].

In the course of collision, the strong interaction region is passed twice for approaching and receding atomic nuclei. The nonadiabatic transition probability for the double passage is [16,19,22]

$$P = 4p(1-p)\sin^2\Phi, \tag{10}$$

$$\Phi = \Delta\Phi - \chi, \quad \Delta\Phi = \Phi_b - \Phi_a, \tag{11}$$

$$\Phi_j(E) = \int_{R_{tj}}^{R_c} \sqrt{2m_{dt}[E - U_j(R)]}\, dR, \tag{12}$$

$m_{dt} = m_d m_t/(m_d + m_t)$. Here Φ_a and Φ_b are the phases gained in adiabatic propagation along the potential curves $U_a(R)$ and $U_b(R)$, respectively, between R_c and the turning points R_{ta} and R_{tb}. The latter are solutions of the equations $U_j(R_{tj}) = E$. We consider head-on collisions (zero impact parameter) that correspond to the total orbital momentum of the system $L = 0$.

An additional so-called dynamic phase χ is gained in the domain of strong nonadiabatic coupling $R \approx R_c$. According to the book by Nikitin and Umanskii [19], this phase is expressed as

$$\chi = [\sqrt{2} - \ln(\sqrt{2}+1)]\frac{\Delta E}{\alpha v}. \tag{13}$$

Below we employ the adiabatic potentials U_a and U_b that are provided by the calculations in the hyperspherical approach [14]. In the hyperspherical method the adiabatic potentials are constructed for fixed values of the hyperradius ρ,

$$\rho = \sqrt{(m_d r_d^2 + m_t r_t^2 + m_\mu r_\mu^2)}, \tag{14}$$

where the vectors $\mathbf{r}_d$, $\mathbf{r}_t$, and $\mathbf{r}_\mu$ define positions of the particles in the center-of-mass frame. It is easy to see that neglecting a term of the order m_μ/m_d, one can approximately relate ρ to the distance R between the nuclei d and t:

$$\rho \approx \sqrt{\frac{m_{dt}}{m_\mu}} R = 3.26R. \tag{15}$$

In terms of the hyperradius the phases are presented as

$$\Phi_j(E) = \int_{\rho_{tj}}^{\rho_c} \sqrt{2m_\mu[E - U_j(\rho)]}\, d\rho. \tag{16}$$

The adiabatic hyperspherical potential curves correlated to the separated atom states with $n_i = 1$ and $n_f = 1$ are shown in Fig. 1. The exchange interaction (9) between two $1s$ states is $H_{1s1s} = 2R\exp(-R-1)$. The energy defect ΔE is given by formula (2) with $n = 1$. Using Eq. (5) we estimate $R_c = 7.11$ (i.e., $\rho_c = 23.18$). Figure 2 shows the phases $\Phi_a(E)$ and $\Phi_b(E)$ and their difference $\Delta\Phi(E)$. One can see that although both $\Phi_a(E)$ and $\Phi_b(E)$ exhibit substantial energy dependences, their difference is almost constant. The transition probability P_{1s1s} calculated according to formula (10) is shown in Fig. 3(a) together with the results of high-precision calculations [14]. The quantum counterpart of P_{1s1s} is $|S_{1s1s}|^2$, where S_{if} is element of scattering matrix. There is a

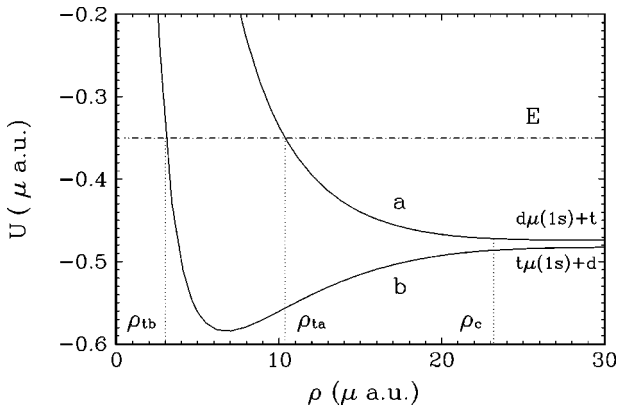

FIG. 1. Two lowest potential curves for $dt\mu$ system as a function of the hyperradius ρ for total orbital momentum $L = 0$. Zero energy corresponds to the threshold of the three-particle breakup. The point of localization of strong nonadiabatic transitions ρ_c is shown together with the turning points ρ_{ta} and ρ_{tb} for the motion along upper (a) and lower (b) adiabatic potential curves for some energy E.

reasonably good agreement between model and numerical results, particularly concerning the energy dependence of the probability, though its absolute value is somewhat underestimated by the model. In Fig. 3(b) we show how the single passage probability (6) depends on the energy E. With increasing E it rapidly approaches the asymptote $p = \frac{1}{2}$ that corresponds to the diabatic limit. The product $2p(1-p)$ approaches the same limit $\frac{1}{2}$ even faster. The latter product is just the reaction probability that would be anticipated if the interference effects were to be discarded, i.e., $\sin^2\Phi$ replaced by its average value $\frac{1}{2}$. However, in fact the reaction probability is strongly suppressed by destructive interference since $\sin^2\Phi$ is very small (Φ proves to be close to 2π). The dynamic phase χ is small in the diabatic regime; taking account of it somewhat enhances the reaction probability, as seen from Fig. 3(a).

B. Rearrangement between excited states: $n_i = 2 \Rightarrow n_f = 2$

There are two Σ potential curves converging to each of separated atom states $d\mu(n_i = 2) + t$ and $d + t\mu(n_f = 2)$. For large internuclear separations R these states correspond to the muonic atom Stark states. The related potential curves at large separations are governed by the charge-dipole interaction. Therefore, they are shifted by $\pm 3/R^2$ relative to the separated atom ($R \to \infty$) limit. We denote these states as $a_\pm$ and $b_\pm$, where the label a is ascribed as before to the initial $d\mu(n_i = 2)$ state and the label b to the final $t\mu(n_f = 2)$ states. The index + (−) labels the states shifted upwards (downwards) on the energy scale by the charge-dipole interaction with incident ion. The potential curves in the hyperspherical basis are shown in Fig. 4.

Thus we have *four* interacting states. In order to identify the most efficient rearrangement transitions we compare coupling $H_{ab}(R)$ between some particular states a and b with the related difference $\Delta E_{ab}^{(L)}(R)$ of diagonal elements of the Hamiltonian matrix in the diabatic basis. These diagonal el-

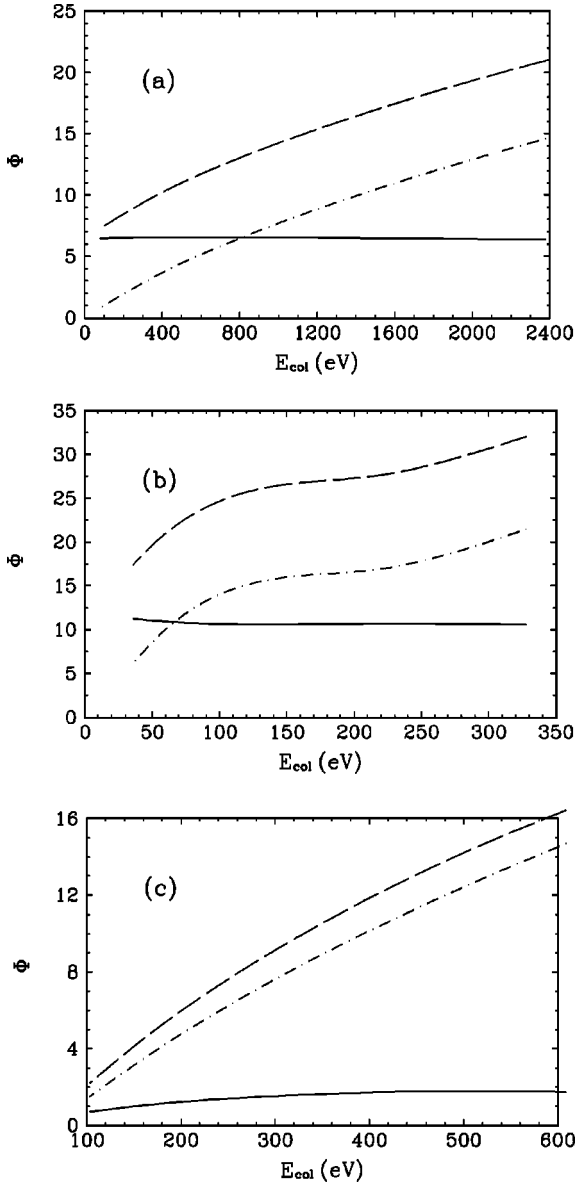

FIG. 2. Interference phases for $1s \to 1s$ (a), and for the Stark states in the $n=2$ manifold: $a_- \to b_-$ (b) and $a_+ \to b_+$ (c) (see text for details). Dash-dotted curve—the phase Φ_a gained in adiabatic propagation along the entrance potential curve $U_a(\rho)$; dashed curve—the same for the exit channel $U_b(\rho)$; solid curve—the phase difference $\Delta\Phi = \Phi_b - \Phi_a$ [see Eqs. (10)–(12)]. $E_{\rm col}$ is the collision energy in the entrance channel.

ements include the long-range part of the interaction that is not related to the particle rearrangement (in the case of a $1s$-$1s$ reaction, the long-range part of the interaction is negligible, being governed by polarization forces). In particular, for the interaction between a_+ and b_- states one has

$$\Delta E^{(L)}_{a_+ b_-}(R) = \Delta E_2 + \frac{6}{R^2}. \tag{17a}$$

For the interaction of pair a_- and b_+, one has

$$\Delta E^{(L)}_{a_- b_+}(R) = \Delta E_2 - \frac{6}{R^2}, \tag{17b}$$

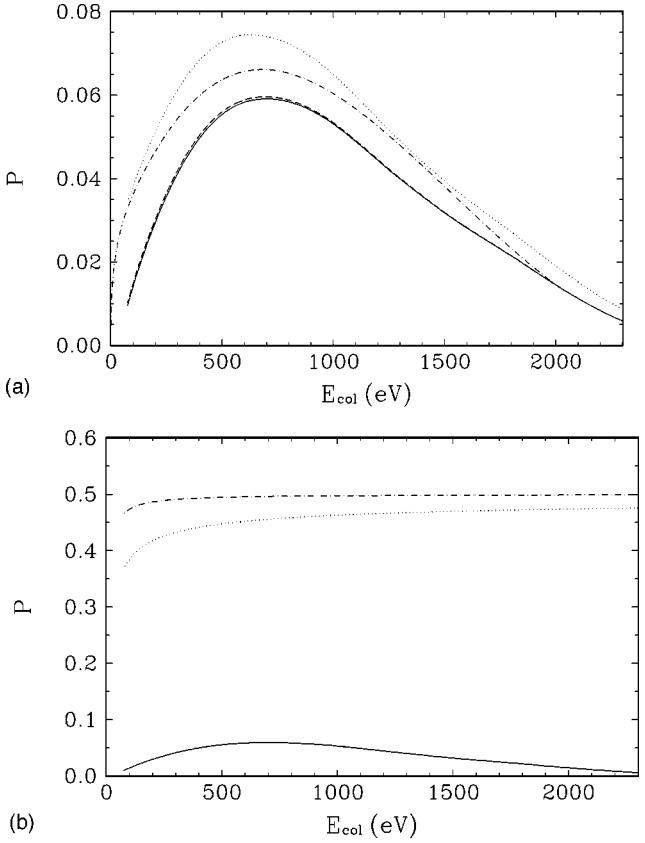

FIG. 3. (a) Model probability of the $d\mu(1s)+t \to d+t\mu(1s)$ reaction (solid curve) and its quantum counterpart $|S_{1s1s}|^2$ obtained in the high-precision calculations (dot-dashed curve). $E_{\rm col}$ is the collision energy in the entrance channel. The dotted curve shows the model probability evaluated neglecting the dynamic phase χ [Eq. (13)]. The dashed curve, almost coinciding with the solid one, presents $\sin^2\Phi$. (b) Model single passage probability p [Eq. (6)] (dotted curve), product $2p(1-p)$ (dash-dotted curve) and model reaction probability [solid curve; same as in (a)].

where ΔE_2 is given by Eq. (2) with $n=2$. For the pairs (a_+, b_+) and (a_-, b_-) the long-range level splitting is not operative: $\Delta E^{(L)}_{a_+ b_+}(R) = \Delta E^{(L)}_{a_- b_-}(R) = \Delta E_2$.

Equation (5) is to be modified [16,21] in order to account

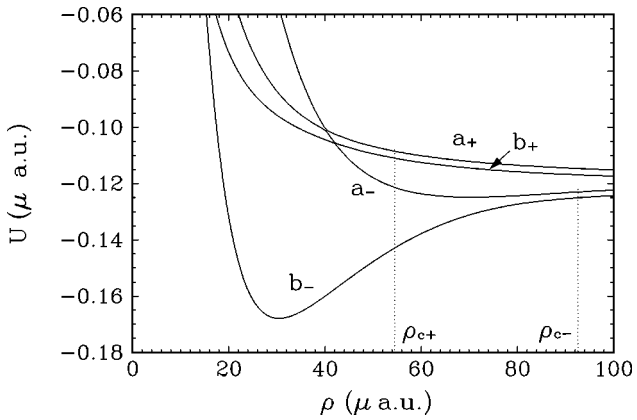

FIG. 4. Same as in Fig. 1, but for four higher-lying potential curves which converge to $d\mu(n_i=2)$ and $d\mu(n_f=2)$ separated atom limits.

for the long-range interaction:

$$|\Delta E_{ab}^{(L)}(R_c)| = 2H_{12}(R_c). \tag{18}$$

Now we have to evaluate the exchange coupling $H_{ab}(R)$ for various pairs of states. The Stark states for $n=2$ are

$$|\pm\rangle = \frac{1}{\sqrt{2}}(|2s\rangle \pm |2p\sigma\rangle). \tag{19}$$

Here $|2p\sigma\rangle$ is the $2p$ state with a zero orbital momentum projection on the internuclear $(d-t)$ axis. Taking the well-known expressions for $2s$ and $2p$ states, and using formulas (9) and (19), we obtain asymptotes of exchange interaction between the Stark states:

$$H_{a_-b_-}(R) = \frac{1}{2}R^3 \exp\left(-\frac{1}{2}R - 2\right), \tag{20a}$$

$$H_{a_-b_+}(R) = H_{a_+b_-}(R) = R^2 \exp\left(-\frac{1}{2}R - 2\right), \tag{20b}$$

$$H_{a_+b_+}(R) = 2R \exp\left(-\frac{1}{2}R - 2\right). \tag{20c}$$

The transition probability (6) is to be evaluated by substituting $\Delta E_2^{(L)}(R_c)$ as ΔE. This magnitude proves to be much larger than ΔE_2 for (a_+, b_-) and (a_-, b_+) pairs. Therefore, the rearrangement transitions within these pairs are strongly suppressed. In simple terms this means that the long-range interaction effectively induces an additional splitting of the related potential curves which is large as compared with the process energy defect ΔE_2. The enhancement of the splitting suppresses the reaction probability. The reaction can effectively proceed only between pairs of potential curves where the long-range splitting is absent, i.e., within (a_+, b_+) and (a_-, b_-) pairs.

The transition point for the (a_-, b_-) pair $R_{c-} = 28.4$ $(\rho_{c-} = 92.56)$ corresponds to substantially larger internuclear separations than for the (a_+, b_+) pair $(R_{c+} = 16.7,\ \rho_{c-} = 54.48)$. This stems from the fact that the coupling [Eq. (20a)] for the former pair is $\frac{1}{4}R^2$ times larger than the coupling [Eq. (20c)] in the latter case. The origin of this feature is clear. The $(-)$ Stark states are shifted downwards in energy because the muonic cloud is stretched towards an approaching collision partner which is a bare atomic nucleus (t in the initial state or d in the final state). The *same effect* enhances the exchange coupling H_{12}, since it is proportional to the overlap of the initial- and final-state electron wave functions at the midpoint between the nuclei, as discussed below Eq. (9). The similar situation was revealed previously [32,33] in a discussion of charge exchange between $\mathrm{Na}(3p) + \mathrm{H}^+ \rightarrow \mathrm{Na}^+ + \mathrm{H}(n=2)$.

Thus the efficient reactive transitions are operative only within (a_-, b_-) and (a_+, b_+) pairs of Stark states. The related probabilities P_- and P_+ evaluated using Eq. (10) are shown in Fig. 5(b). The single-passage probability p [Eq. (6)] was calculated with collision velocity $v = v_{c\pm}$ evaluated at the transition point

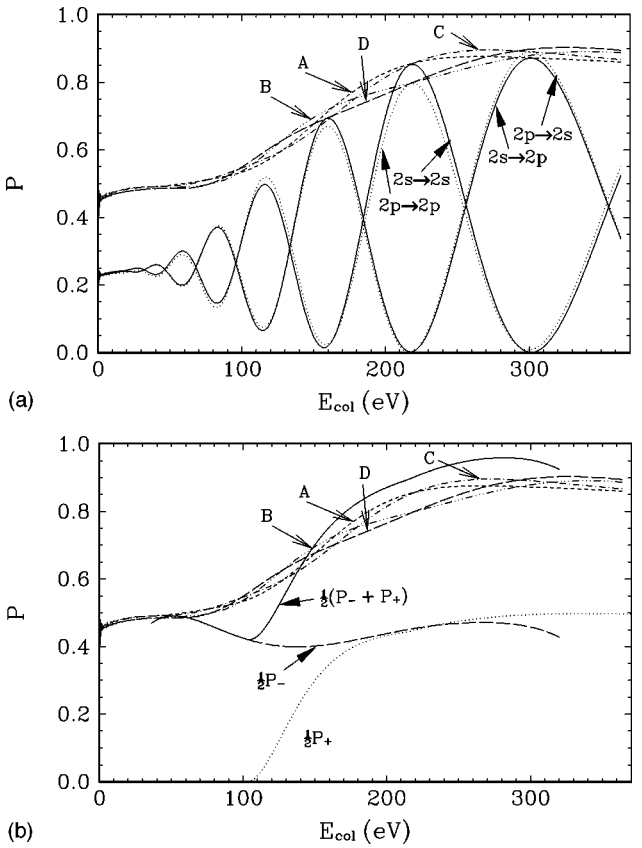

FIG. 5. (a) Qualitative features in the transfer probabilities obtained in high-precision quantum calculations [14] for the reaction $d\mu(n_i=2) + t \rightarrow d + t\mu(n_f=2)$. E_{col} is the collision energy in the entrance channel. The approximate equalities $P_{2s2s} \approx P_{2p2p}$ [Eq. (23a)] and $P_{2s2p} \approx P_{2p2s}$ [Eq. (23b)] make the related curves very close on the plot scale (note that the probabilities with initial $2s$ and $2p$ states are shown by dotted and solid curves, respectively). In agreement with Eq. (24), a tight bunch is formed by four curves representing pairwise sums of transfer probabilities, namely, $P_{2s2s} + P_{2s2p}$ (A, short-dashed curve), $P_{2s2s} + P_{2p2s}$ (B, dot-dot-dashed curve), $P_{2p2p} + P_{2s2p}$ (C, dot-dashed curve), and $P_{2p2p} + P_{2p2s}$ (D, long-dashed curve). (b) Model probability of reaction $d\mu(n_i=2) + t \rightarrow d + t\mu(n_f=2)$ compared with high-precision results. Four curves A–D [the same as in (a)] in the model approach correspond to a single solid curve, which is the sum $\frac{1}{2}(P_- + P_+)$. The effective reaction channel contributions $\frac{1}{2}P_-$ and $\frac{1}{2}P_+$ are also shown.

$$v_{c\pm} = \sqrt{\frac{2E - [U_a(\rho_{c\pm}) + U_b(\rho_{c\pm})]}{\mathcal{M}_i}}. \tag{21}$$

For transitions within $n_i = n_f = 1$ the difference between v [Eq. (7)] and v_c is negligible. In the present case this difference is substantial, leading to important features. Since a_- and b_- potential curves correspond to attraction, the heavy particles are accelerated as they approach each other, and hence the transition probability P_- remains finite as collision energy tends to zero, in contradistinction with $n_i \Rightarrow n_f = 1$ transitions where the probability tends to zero. Moreover,

repulsive a_+ and b_+ potential curves lead to heavy particle deceleration, and the (a_+,b_+) transitions become substantial only provided the collision energy is sufficiently high $[E > U_a(\rho_{c+}) \sim U_b(\rho_{c+})]$. This is the reason for the appearance of an effective threshold for the P_- probability at $E_{\rm col} \approx 105$ eV. The interference phases Φ_- and Φ_+ exhibit only a weak energy dependence similar to the $1s$-$1s$ case discussed above. Distinct from the latter case, we now have constructive interference, $\sin^2\Phi_\pm$ being close to unity for both $(+)$ and $(-)$ Stark channels in a broad interval of collision energies. The neglect by the dynamic phase χ almost does not change the model probabilities in the scale of Fig. 5(b) (not shown). Within the same accuracy the model probabilities coincide with the factors $\sin^2\Phi_\pm$ (also not shown). These features are due to a diabatic regime that is operative in the energy domain considered (cf. Sec. II A).

In Fig. 5(a) squared moduli $P_{if} \equiv |S_{if}|^2$ of S-matrix elements for the reaction obtained in high-precision calculations [14] are presented in terms of initial and final states labeled by the spherical quantum numbers (namely, $2s$ and $2p$ states). The strong suppression of transitions within (a_+,b_-) and (a_-,b_+) pairs means that in the *Stark basis* one has

$$S_{a_+b_-} \approx S_{a_-b_+} \approx 0. \tag{22}$$

From this we obtain

$$P_{2s2s} \approx P_{2p2p} \approx |S_{a_-b_-} + S_{a_+b_+}|^2 \tag{23a}$$

and

$$P_{2s2p} \approx P_{2p2s} \approx |S_{a_-b_-} - S_{a_+b_+}|^2. \tag{23b}$$

As can be seen from Fig. 5(a), these approximate equalities indeed hold rather well, which gives an independent confirmation of the decoupling (22). Next, from Eqs. (23), we obtain:

$$P_{2s2s} + P_{2s2p} \approx P_{2s2s} + P_{2p2s} \approx P_{2p2p} + P_{2s2p} \approx P_{2p2p} + P_{2p2s} \approx \frac{1}{2}(P_- + P_+), \tag{24}$$

where $P_\pm = |S_{a_\pm b_\pm}|^2$. The accurate results for the first four expressions here are shown by curves A–D in Fig. 5(a). According to Eq. (24), these curves must approximately coincide with each other, which is indeed the case. The expression in the last line in Eq. (24) evaluated according to the Demkov model is plotted in Fig. 5(b) by a solid line. This curve reproduces the major features of accurate results: it is close to 0.5 at small collision energy and in the interval 100 eV$<E_{\rm col}<$200 eV rises to values somewhat lower than unity. The largest deviations are observed near the effective threshold of the $(+)$ channel, apparently because the present model neglects tunneling transitions below the threshold. As stated in Sec. I, the development of more sophisticated models is beyond the scope of the present study.

Figure 5(a) demonstrates that P_{2s2s} and P_{2s2p} oscillate in antiphase as functions of the collision energy E, whereas the sum over final states $P_{2s2s}+P_{2s2p}$ exhibits a smooth energy dependence. The same situation is observed for the probabilities P_{2p2s} and P_{2p2p} and their sum. The explanation for this fact is obvious [11]. The $2s$ and $2p$ states are linear combinations of $(+)$ and $(-)$ Stark states. Therefore, the relative phases of the final $(+)$ and $(-)$ Stark states are important to calculate transitions into the spherical states. The magnitude of these phases is governed mostly by the long-range charge-dipole interaction. It changes rapidly with collision energy, and induces interference oscillations in the probability distribution over the final $2s$ and $2p$ states seen in Fig. 5(a). In this study we do not aim to reproduce these oscillations, being interested mostly in a bulk evaluation of the reaction efficiency.

At smaller ρ the a_- potential curve is strongly promoted, and crosses the a_+ and b_+ potential curves at $\rho \approx 40-41$ (see Fig. 4) (for b_- curve similar crossings occur at even smaller ρ and higher energies not shown in Fig. 4). In fact there are curve pseudocrossings, but with splittings so small that they could not be discerned on the scale of Fig. 4. Therefore these pseudocrossings are passed diabatically and do not play any role in the transition dynamics. This conclusion is at variance with that done by Hino and Macek [11], who interpreted results of their numerical calculation in terms of such a pseudocrossing.

III. DISCUSSION. INTERFERENCE PHASES

Process (1) is a particular case of light particle exchange between two heavy particles with a small energy defect. Its prototypes are well studied in atomic physics. However, reaction (1) has two generic features: (a) the energy defect has a purely isotopic nature; and (b) the excited states of separated atoms are degenerate in orbital momentum both in entrance and exit channels.

The analysis of Sec. II shows that the Demkov model works rather well for the studied cases. The model applicability was tested for the partial rearrangement cross sections in the case when the system has zero total orbital momentum L. Only for this case were high-precision calculations carried out (see Ref. [14], where a comparison with earlier calculations was considered in detail). This, of course, is not accidental since in the general case $L \neq 0$ some additional substantial problems appear in high-precision quantum calculations. The model approach, albeit less accurate, does not meet such difficulties. It is easily extendable to arbitrary L, and hence to an evaluation of the total rearrangement cross sections. To illustrate this, in Fig. 6 we present the total cross sections of the $1s \Rightarrow 1s$ rearrangement as a function of the collision energy $E_{\rm coll}$. A well-known formula of semiclassical nature was employed,

$$\sigma = 2\pi \int_0^{R_0} P(b)\, b\, db, \tag{25}$$

where the rearrangement probability $P(b)$ [Eq. (10)] is now a function of impact parameter b ($L=kb$, k is the wave number). This dependence enters, first, via the formulas (6) and (13), where v is to be understood as the radial col-

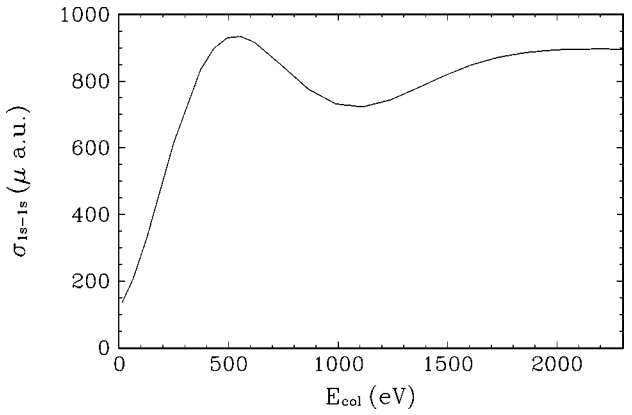

FIG. 6. Total cross section of $1s \Rightarrow 1s$ rearrangement process (1) as a function of collision energy $E_{\rm coll}$.

lision velocity at the transition point $R=R_0$ [$v=\sqrt{2E_{\rm coll}(1-b^2/R_0^2)/\mathcal{M}_i}$]. Second, in a calculation of the phases Φ_j [Eq. (12)], one has to account for the effective centrifugal repulsion by replacing $U_j(R)$ with $U_j(R)+E_{\rm coll}b^2/R^2$.

No less important is a conceptual side, namely, a clarification of the mechanisms of reaction (1) between states of the $n_i=n_f=1$ and $n_i=n_f=2$ manifolds. The reaction occurs via nonadiabatic transitions in localized regions via the Demkov mechanism. The multistate case of the $n_i=2 \Rightarrow n_f=2$ rearrangement is particularly interesting. The oscillatory energy dependence of the state-to-state transition probabilities together with other particular features [as expressed by our Eqs. (23)] were noticed in the numerical calculations [14], but the interpretation was left for the model approach. The latter effectively reduces the four-state problem to two pairwise Demkov-type transitions. One of them has a higher effective threshold than the other, that was physically interpreted in Sec. II. The present study confirms the validity of the Demkov model for treating quasiresonance rearrangement processes in the situation where the energy defect has a purely isotopic nature.

Interference effects are neglected in many studies which amounts to replacing the $\sin^2\Phi$ factor in Eq. (10) by its average value $\frac{1}{2}$. The averaging is usually meant to go over the impact parameter (see, for instance, the recent applications to the muon transfer problem [8,13]). We do not resort to this approximation in our calculations of the total cross section (25). Of course, there are no reasons for this when the particular partial wave $L=0$ is considered. Our analysis demonstrates the crucial importance of interference effects that strongly suppress the reaction probability in the case of $1s \Rightarrow 1s$ transitions, and enhance it to almost unity in the case of $n_i=2 \Rightarrow n_f=2$ transitions. In fact it is the $\sin^2\Phi$ factor that essentially defines the energy dependence of the reaction probability (10). Note that a description of interference effects requires a knowledge of adiabatic potential curves in a broad range of ρ (or R); otherwise a large-R asymptotic approach is sufficient to estimate the Demkov model parameters.

There is also another surprising property of the interference phases to be discussed here. In Fig. 2 we show the

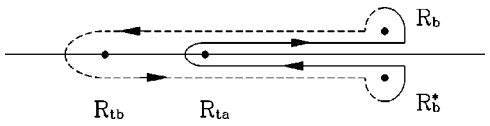

FIG. 7. Branch points R_b and R_b^*, turning points R_{ta} and R_{tb}, and integration contour in the complex R plane for evaluation of the interference phase [Eq. (27a)].

energy dependence of the adiabatic phases Φ_a and Φ_b defined by Eq. (16), and their difference $\Delta\Phi=\Phi_b-\Phi_a$ for all three studied cases. As can be seen from the figure, while phases $\Phi_{a,b}$ vary considerably, their difference $\Delta\Phi$ demonstrates a much weaker dependence on the collision energy, being approximately equal to 2π for the case $n_i=n_f=1$, $\frac{7}{2}\pi$ for the $(-)$ states of the $n_i=n_f=2$ manifold, and rapidly rising to $\frac{1}{2}\pi$ and then stabilizing for the $(+)$ states. We consider $\Delta\Phi$ instead of Φ because this phase has a more clear physical meaning and because the dynamical phase χ is small except in the near-threshold regions, so that $\Delta\Phi \approx \Phi$.

The very weak dependence of the interference phase $\Delta\Phi$ on the collision energy is a quite unexpected and intriguing fact. It can be cast as an approximate isochronous property, i.e., the equality of time needed for the system to travel from the point R_c to the turning points R_{ta} or R_{tb} along each of two adiabatic states concerned:

$$T_1(E) \approx T_2(E), \quad T_j(E)=\sqrt{\frac{m_{dt}}{2}}\int_{R_{ij}}^{R_c}\frac{dR}{\sqrt{E-U_j(R)}} = \int_{\rho_{tj}}^{\rho_c}\frac{d\rho}{\sqrt{2[E-U_j(\rho)]}}. \tag{26}$$

The interference phase $\Delta\Phi$ can be represented by an integral over a closed contour in the complex-R plane. This possibility is based on the observation that the potential curves $U_j(R)$ are different branches of a unique multivalued analytical function $U(R)$ of complex R (this idea was originally put forward by Demkov [34], and extensively developed and applied by Solov'ev [35]). This concept leads to a viewpoint of collision dynamics as traveling on the multivalued potential-energy surface being the essence of the so-called hidden-crossing theory. The transition from one potential curve to another is achieved by following some path in the Riemann surface that encircles the *branch point* R_b. Two branch points R_b and R_b^* are essential in the present case with $\mathrm{Re}\,R_b$ close to $R_c(\mathrm{Im}\,R_b \ll R_c)$. The phase difference is cast as an integral

$$2\,\Delta\Phi(E)=\oint_{\mathcal{C}}\sqrt{2m_{dt}[E-U_j(R)]}dR \tag{27a}$$

or

$$2\,\Delta\Phi(E)=\oint_{\mathcal{C}}\sqrt{2m_{\mu}[E-U_j(\rho)]}d\rho \tag{27b}$$

over the contour $\mathcal{C}$ schematically shown in Fig. 7. The contour goes from the initial to final sheet encircling R_b, and

then returns, encircling R_b^*. It hooks on the turning points R_{ta} and R_{tb} that also are branch points of the integrand. The importance of the contour integral representation stems from the fact that it casts the phase difference as a basic entity independent of any model. It is invariant under deformations of the contour (without crossing integrand singularities), and characterizes properties of the potential curve as a multivalued analytical function.

Strictly speaking, the branch point R_b does not belong to the series discussed in the hidden crossing theory where two heavy particles are considered as space-fixed centers of force, and thus the isotopic effects are not included. Indeed, if the isotopic effects are ''switched off,'' then one has $\Delta E_n \to 0$ and $R_b \to +\infty$. However, one can presume that the small difference of the heavy particle masses could be mimicked by a small difference of the charges, that is, in the spirit of Sec. II. Then the branch points emerging in the present study belong to the Q series studied in the hidden crossings framework [23]. In practical applications of the hidden-crossing theory, till now phase effects were mostly ignored, with some rare exceptions [36]. Perhaps a subsequent development of this theory would be able to explain the properties of the interference phases discussed above. In conclusion, we also note that the model approach discussed in this paper can be extended to higher manifolds that may result in a simple method for estimating cumulative reaction probability [12].

Note added in proof. Recently, the article by S. J. Ward, J. H. Macek, and S. Yu. Ovchinnikov appeared [Phys. Rev. A **59**, 4418 (1999)]. These authors applied the hidden-crossing theory to study the rearrangement process in another three-body Coulomb system, e^+e^-p. In particular, they found that for S scattering the interference phase in the ground-to-ground rearrangement channel is close to π, in agreement with our result in Sec. II A. Additionally, for D scattering the phase proved to be about $\frac{1}{2}\pi$. The rearrangement between excited states was not considered in the cited publication.

ACKNOWLEDGMENTS

I am thankful to O. I. Tolstikhin for providing results of his calculations prior to publication, and for many enlightening discussions. This work was initiated during my stay at The Institute for Molecular Sciences in Okazaki supported by the Ministry of Education, Science, Culture, and Sports of Japan. I am indebted to H. Nakamura for support, hospitality, and much useful advice.

[1] K. Kobayashi, T. Ishihara, and N. Toshima, Muon Catal. Fusion **2**, 191 (1988).
[2] M. Kamimura, Muon Catal. Fusion **3**, 335 (1988).
[3] H. Fukuda, T. Ishihara, and S. Hara, Phys. Rev. A **41**, 145 (1990).
[4] J. S. Cohen and M. C. Struenee, Phys. Rev. A **43**, 3460 (1991).
[5] C. Chiccoli, V. I. Korobov, V. S. Melezhik, P. Pasini, L. I. Ponomarev, and J. Wozniak, Muon Catal. Fusion **7**, 87 (1992).
[6] Y. Kino and M. Kamimura, Hyperfine Interact. **82**, 45 (1993).
[7] V. V. Gusev, L. I. Ponomarev, and E. A. Solov'ev, Hyperfine Interact. **82**, 53 (1993).
[8] W. Czapliński, A. Gula, A. Kravtsov, A. Mikhailov, and N. Popov, Muon Catal. Fusion **5/6**, 59 (1990/91); Phys. Rev. A **50**, 518 (1994); **50**, 525 (1994).
[9] A. Igarashi, N. Toshima, and T. Shirai, Phys. Rev. A **50**, 4951 (1994).
[10] A. A. Kvitsinsky, C. Y. Hu, and J. S. Cohen, Phys. Rev. A **53**, 255 (1996).
[11] K. Hino and J. H. Macek, Phys. Rev. Lett. **77**, 4310 (1996).
[12] O. I. Tolstikhin, V. N. Ostrovsky, and H. Nakamura, Phys. Rev. Lett. **80**, 41 (1998).
[13] L. I. Ponomarev and E. A. Solov'ev, Pis'ma Zh. Eksp. Teor. Fiz. **68**, 9 (1998) [JETP Lett. **68**, 7 (1998)].
[14] O. I. Tolstikhin and C. Namba, Phys. Rev. A **60**, 5111 (1999).
[15] See, e.g., L. I. Ponomarev, Contemp. Phys. **31**, 219 (1990); J. S. Cohen, in *Review of Fundamental Processes and Applications of Atoms and Ions*, edited by C. D. Lin (World Scientific, Singapore, 1993), p. 61.
[16] Yu. N. Demkov, Zh. Eksp. Teor. Fiz. **45**, 195 (1963) [Sov. Phys. JETP **18**, 138 (1964)].
[17] N. Rosen and C. Zener, Phys. Rev. **40**, 502 (1932).
[18] W. E. Mayerhof, Phys. Rev. Lett. **31**, 1341 (1973).
[19] E. E. Nikitin and S. Ya. Umanskii, *Theory of Slow Atomic Collisions* (Berlin, Springer, 1984).
[20] R. K. Janev, L. P. Presnyakov, and V. P. Shevelko, *Physics of Highly Charged Ions* (Springer, Berlin, 1985).
[21] F. F. Karpeshin and V. N. Ostrovsky, J. Phys. B **14**, 4513 (1981).
[22] H. Nakamura, Chem. Phys. Lett. **141**, 77 (1987); Adv. Chem. Phys. **LXXXII**, 243 (1992); A. Ohsaki and H. Nakamura, Chem. Phys. Lett. **142**, 37 (1987).
[23] R. K. Janev, Phys. Rev. A **55**, R1573 (1997); **55**, 4285 (1997).
[24] Yu. N. Demkov, D. F. Zaretskii, F. F. Karpeshin, M. A. Listengarten, and V. N. Ostrovsky, Pis'ma Zh. Eksp. Teor. Fiz. **28**, 287 (1978) [JETP Lett. **28**, 263 (1978)].
[25] D. F. Zaretskii, F. F. Karpeshin, M. A. Listengarten, and V. N. Ostrovsky, Yad. Fiz. **31**, 47 (1980) [Sov. J. Nucl. Phys. **31**, 24 (1980)].
[26] L. I. Menshikov, Zh. Eksp. Teor. Fiz. **85**, 1159 (1983) [Sov. Phys. JETP **58**, 675 (1983)].
[27] V. I. Osherov and A. I. Voronin, Phys. Rev. A **49**, 265 (1994).
[28] O. I. Tolstikhin, S. Watanabe, and M. Matsuzawa, Phys. Rev. Lett. **74**, 3573 (1995); *The Physics of Electronic and Atomic Collisions*, edited by L. J. Dubé, J. B. A. Mitchell, J. W. McConkey, and C. E. Brion, AIP Conf. Proc. No. 360 (AIP, New York, 1995), p. 887.
[29] O. I. Tolstikhin, S. Watanabe, and M. Matsuzawa, J. Phys. B **29**, L389 (1996).
[30] K. L. Baluja, P. G. Burke, and L. A. Morgan, Comput. Phys. Commun. **27**, 299 (1982).
[31] M. I. Chibisov and R. K. Janev, Phys. Rep. **166**, 1 (1988).
[32] V. N. Ostrovsky, Phys. Rev. A **49**, 3740 (1994).
[33] Y. Wang, J. Westphal, Z. Roller-Lutz, V. N. Ostrovsky, and H. O. Lutz, Z. Phys. D **30**, 217 (1994).

[34] Yu. N. Demkov, in *The Physics of Electronic and Atomic Collisions, Leningrad 1967*, Invited Papers of the XI International Conference on The Physics of Electronic and Atomic Collisions, edited by I. P. Flaks and E. A. Solov'ev (Joint Institute for Laboratory Astrophysics, Boulder, CO, 1968), p. 186.

[35] E. A. Solov'ev, Usp. Fiz. Nauk **157**, 437 (1989) [Sov. Phys. Usp. **32**, 228 (1989)].

[36] R. K. Janev, J. Pop-Jordanov, and E. A. Solovyov, J. Phys. B **30**, L353 (1997).